Synthetic ionophores. Part 18: Ag⁺ selective trithiabenzena- and dithiabenzenapyridinacyclophanes [1]

Subodh Kumar,* Maninder Singh Hundal, Geeta Hundal, Palwinder Singh, Vandana Bhalla and Harjit Singh*

Department of Chemistry, Guru Nanak Dev University, Amritsar 143 005, India

The phase transfer catalysed nucleophilic displacement of 1,3-bis(bromomethyl)benzene, 2-methoxy-5-methyl-1,3-bis(bromomethyl)benzene (2) and 1,4-bis(bromomethyl)benzene with 2-mercaptoethanol gives the respective diols 3, 4 and 12 (80–85%), which undergo intermolecular cyclodehydrochlorination with thiodiglycolyl dichloride and pyridine-2,6-dicarbonyl dichloride·HCl to provide *m*-phenylene (7–10) and *p*-phenylene (13–14) based crownophanes. The single crystal X-ray structures of crownophanes 8 and 13 and their NMR studies show that the *m*-phenylene and *p*-phenylene rings remain in plane and perpendicular to the macrocyclic ring both in solution and solid phases. These crownophanes offer three soft coordinating sites (3 × S or 2 × S and 1 N) conducive to complexation with Ag⁺ and the steric restrictions imposed by *m*- and *p*-phenylene rings restrict 2∶1 (L∶M) sandwich complexation required for complexation with the borderline soft Pb²⁺ cation. The crownophanes 7 and 9 extract Ag⁺ 172 and 602 times, respectively, more than Pb²⁺.

Introduction

The development of fast estimation, removal and separation techniques for precious and toxic silver and the use of silver complexes in photographic materials and their potential use in cancer radioimmunotherapy has drawn the attention of supramolecular chemists towards the design, synthesis and evaluation of silver selective ionophores. For designing such ionophores, the optimum requirement of 2–4 soft (S or N) ligating sites [2–7] preorganized in a three-dimensional system has been emphasized. In the reported Ag⁺ selective ionophores, the presence of ether units [8–12] responsible for binding towards hard alkali, alkaline earth and borderline Pb²⁺ cations and the possibility of the formation of sandwich or polymeric complexes [13–15] creating significant binding towards most soft metal ions, cause lowering of Ag⁺ selectivities. We argued that in such hosts, the absence of hard (ether) ligating sites and the presence of stereochemical or structural features which could inhibit their sandwich or polymeric complexation requiring >1∶1 stoichiometric host–guest interaction could further enhance the Ag⁺ selectivity even against the similar sized Pb²⁺ cation. We envisaged that to achieve such an inhibition, the crownophane designs 7–10, 13 and 14 could easily adopt the edge-on arrangement of *m*- and *p*-phenylene rings with respect to the plane of the macrocyclic ring especially during complexation. Here, we have reported the synthesis and evaluation of these ionophores and have found that *m*-phenylene derivatives 7 and 9 show a high order of selectivity for Ag⁺.
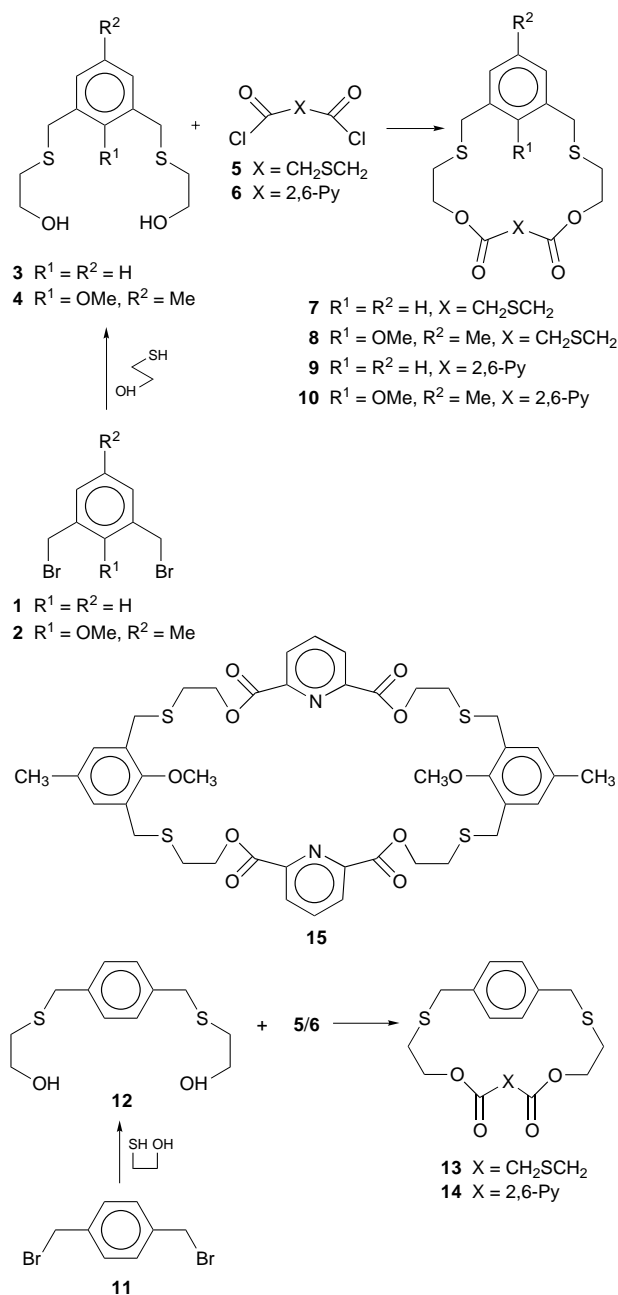
Results and discussion

Synthesis

For the synthesis of crownophanes 7–10, 13 and 14, the two step approach involving the reactions of appropriate dihalides with 2-mercaptoethanol to form diols (3, 4 and 12) followed by their intermolecular cyclodehydrochlorination with appropriate diacid dichlorides was adopted. The phase transfer catalysed (K₂CO₃–DMF–Bu₄N⁺HSO₄⁻) nucleophilic displacement of 1,3-bis(bromomethyl)benzene (1) with 2-mercaptoethanol gave diol 3 (80%), *m/z* 258. Similarly, reactions of 2-methoxy-5-methyl-1,3-bis(bromomethyl)benzene (2) and 1,4-bis(bromomethyl)benzene (11) with 2-mercaptoethanol under these phase transfer catalysis (PTC) conditions gave diols 4 (80%), *m/z*

286 and 12 (85%), mp 58 °C, *m/z* 258, respectively. The slow addition of thiodiglycolyl dichloride to a solution of 3 containing KF (anhyd.) as base and Bu₄N⁺HSO₄⁻ as catalyst provided macrocycle 7 (40%), liquid, *m/z* 372. Similarly, reactions of diols 4 and 12 with thiodiglycolyl dichloride under these PTC conditions gave crownophanes 8 (35%), mp 100 °C, *m/z* 416 and 12 (10%), mp 62 °C, *m/z* 372, respectively. The diols 3, 4 and 12 failed to react with pyridine-2,6-dicarbonyl dichloride·HCl under the above PTC conditions. However, on reacting diols 3 and 12 with 6·HCl by using K₂CO₃ (anhyd.) as base, the crownophanes 9 (35%), mp 147 °C, *m/z* 389, and 14 (25%), mp 197 °C, *m/z* 389, respectively, could be formed. The reaction of diol 4 with 6·HCl under these conditions gave 10 (35%), mp 197 °C, *m/z* 433 along with the 2∶2 stoichiometric product 15 (10%), mp 180 °C, *m/z* (FAB) 867 (M⁺ + 1). A 2∶2 stoichiometric reaction might be triggered in the initial 1∶1 stoichiometric intermediate by steric inhibition of the *para*-substituents of the phenylene ring, in its cyclization.

Conformational analysis

The X-ray crystal structure of crownophane 8 (Fig. 1, Table 1) shows that the *m*-phenylene ring remains in the mean plane of the macrocyclic ring. The substituent O–Me seems to play a dominant role in determining the conformation of the macroring. The bond O5–C18 is almost perpendicular to the phenylene ring (C11–C16–O5–C18 being 96.7°). The torsion angle S2–C10–C11–C16 is 86.2(3)° and consequently both S2–C10 and C18–O5 bonds point towards the same side with respect to the phenylene ring (Fig. 1). To avoid steric crowding the S1–C1 bond points in a direction opposite to the C18–O5 bond, the torsion angle C16–C15–C1–S1 being 97.8(3)°. The torsion angle studies indicate that out of the four possible 1,4-thiaoxa units (O–CH₂–CH₂–S), three are antiperiplanar [torsion angles 173.8(2)–177.1(2)°], whereas the fourth one (O4–C8–C9–S3) is synclinal [59.7(3)°] about the C–C bond. The torsion angles about the C–O bond are antiperiplanar and about the C–S bond they are synclinal with the exception of C9–S2–C10–C11 which is antiperiplanar. In the segments O1–C4–O2 and O3–C7–O4, the carbonyl oxygens O2 and O4 point towards opposite sides of the macro-ring mean plane. The major difference in the conformation angles in the two halves of the macro-ring is that torsion angle C2–S1–C1–C15 is synclinal whereas

Fig. 1 ORTEP view of crownophane **8**. Thermal ellipsoids are drawn with 50% probability and hydrogen atoms are drawn with arbitrary small isotopic thermal parameters for the sake of clarity.

Table 1 Selected bond distances and angles for **8** and **13**

	Bond distances/Å		Bond angles/°
Crownophane 8			
S(1)–C(2)	1.798(3)	C(2)–S(1)–C(1)	100.86(13)
S(1)–C(1)	1.821(3)	C(6)–S(3)–C(5)	100.96(13)
S(3)–C(6)	1.793(3)	C(9)–S(2)–C(10)	102.86(14)
S(3)–C(5)	1.796(3)	C(4)–O(1)–C(3)	117.7(2)
S(2)–C(9)	1.811(3)	C(7)–O(3)–C(8)	116.0(2)
S(2)–C(10)	1.811(3)	C(3)–C(2)–S(1)	113.1(2)
O(1)–C(4)	1.334(4)	O(1)–C(3)–C(2)	106.8(2)
O(1)–C(3)	1.455(3)	O(2)–C(4)–O(1)	124.1(3)
O(2)–C(4)	1.199(3)	O(2)–C(4)–C(5)	126.7(3)
O(4)–C(7)	1.195(3)	O(1)–C(4)–C(5)	109.2(3)
O(3)–C(7)	1.333(3)	C(4)–C(5)–S(3)	115.0(2)
O(3)–C(8)	1.453(3)	C(7)–C(6)–S(3)	115.2(2)
O(5)–C(16)	1.394(3)	O(4)–C(7)–O(3)	124.0(3)
O(5)–C(18)	1.429(4)	O(4)–C(7)–C(6)	126.7(3)
		O(3)–C(7)–C(6)	109.3(2)
		O(3)–C(8)–C(9)	109.2(2)
		C(8)–C(9)–S(2)	117.6(2)
		C(11)–C(10)–S(2)	109.5(2)
		C(16)–O(5)–C(18)	115.5(2)
		C(15)–C(1)–S(1)	113.9(2)
Crownophane 13			
S(1)–C(2)	1.792(5)	C(2)–S(1)–C(1)	102.5(2)
S(1)–C(1)	1.808(6)	C(6)–S(3)–C(5)	101.0(3)
S(3)–C(6)	1.792(5)	C(9)–S(2)–C(10)	101.8(2)
S(3)–C(5)	1.803(5)	C(4)–O(1)–C(3)	117.0(4)
S(2)–C(9)	1.801(5)	C(7)–O(3)–C(8)	115.6(4)
S(2)–C(10)	1.810(5)	C(3)–C(2)–S(1)	113.2(3)
O(1)–C(4)	1.343(6)	O(1)–C(3)–C(2)	111.8(4)
O(1)–C(3)	1.437(6)	O(2)–C(4)–O(1)	124.2(5)
O(2)–C(4)	1.192(6)	O(2)–C(4)–C(5)	124.7(6)
O(4)–C(7)	1.201(6)	O(1)–C(4)–C(5)	111.2(6)
O(3)–C(7)	1.327(6)	C(4)–C(5)–S(3)	113.5(3)
O(3)–C(8)	1.451(6)	C(7)–C(6)–S(3)	115.4(4)
O(5)–C(16)		O(4)–C(7)–O(3)	123.6(5)
O(5)–C(18)		O(4)–C(7)–C(6)	125.6(6)
		O(3)–C(7)–C(6)	110.7(5)
		O(3)–C(8)–C(9)	107.6(4)
		C(8)–C(9)–S(2)	112.0(4)
		C(11)–C(10)–S(2)	114.8(3)
		C(16)–O(5)–C(18)	
		C(15)–C(1)–S(1)	

C9–S2–C10–C11 is antiperiplanar, which may be attributed to the steric factors. Three thioether units make a triangle with S1–S2, S2–S3 and S3–S1 placed at 7.13, 6.72 and 7.72 Å.

In the *p*-cyclophane based macrocycle **13** (Fig. 2, Table 1), the phenylene ring and the –CH₂– groups attached at the *para*-positions form one plane and the π-electron cloud of the phenylene ring is almost perpendicular to the macro-ring. Both the sulfur atoms are so oriented that the two bonds C1–S1 and C10–S2 are on the same side of the phenylene ring, in contrast to *m*-cyclophane where these bonds were on the opposite sides of the phenylene ring mean plane due to steric crowding caused by the OMe substituent. Out of the four 1,4-thiaoxa units, three are antiperiplanar and one (O1–C4–C5–S3) is synclinal about the C–C bond (Fig. 2). The two carbonyl oxygens O2 and O4 are present on opposite sides of the marco-ring mean plane, which is also observed in the case of *m*-cyclophane. The torsion angles about C–S are all synclinal and antiperiplanar about C–O except for C4–O1–C3–C2 which is synclinal. This difference in torsion angles about the C–O bonds gives an extended conformation to one side of the macro-ring and introduces a kink at the C2–C3 bond. The three thioether units make a triangle with S1–S2, S2–S3 and S3–S1 placed at 7.15, 7.86 and 6.70 Å.
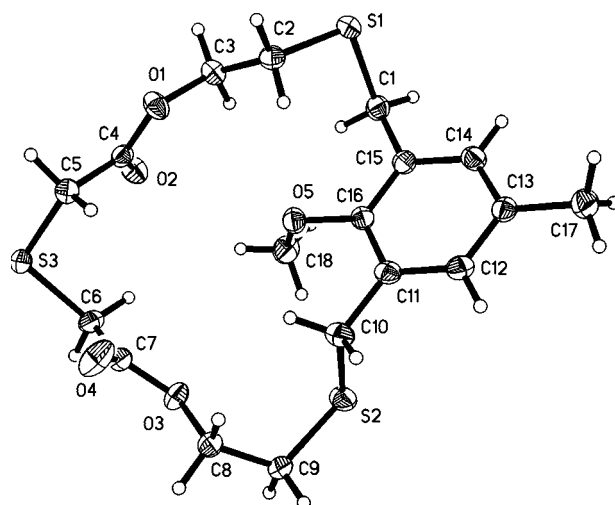
In ¹H NMR spectra, the diols **3**, **4** and **12** show benzylic CH₂, OCH₂ and SCH₂ signals at δ 3.70 (s), 3.63 (t) and 2.60 (t), respectively.[16] In macrocycles **7** and **8**, these signals appear at 3.74, 4.20 and 2.62 respectively and S*CH₂*CO appears at 3.36.

Table 2 Distances and angles between the three coordinating sites in crownophanes **7–10** and **13–14** as calculated from forcefield calculations

	Distances/Å			Angles/°		
Macrocycle	S1–S2	S2–S3/N	S3–S1/N	S1–S2–S3(N)	S2–S3(N)–S1	S3(N)–S1–S2
7	6.57	5.51	6.23	61.40	67.69	50.91
8	6.49	5.51	6.24	62.49	66.33	51.04
13	7.09	3.91	5.08	44.27	103.00	32.40
9	7.24	5.31	4.99	43.59	89.28	47.13
10	7.28	5.30	5.05	43.91	89.39	46.70
14	7.78	5.93	5.03	40.34	90.00	49.66
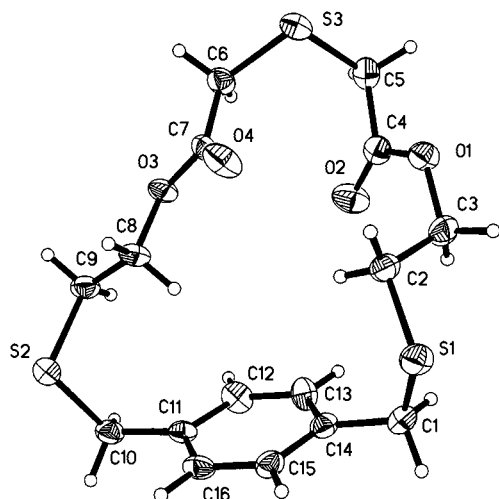
Fig. 2 ORTEP view of crownophane **13**. Thermal ellipsoids are drawn with 50% probability and hydrogen atoms are drawn with arbitrary small isotopic thermal parameters for the sake of clarity.

But in the *p*-crownophane **13**, SCH_2CH$_2$ ($\Delta\delta$ −0.10), SCH_2CO ($\Delta\delta$ −0.20) and OCH_2 ($\Delta\delta$ −0.42) signals are shifted upfield, benzylic CH$_2$ is not affected and ArH appears as a sharp 4H singlet. This upfield shift of signals in **13** in comparison with **7** and **8** clearly shows that in **13**, the *p*-phenylene ring is oriented perpendicular to the plane of the macrocycle, whereas the *m*-phenylene rings of **7** and **8** are in the plane of the crown ring. The planar *p*-phenylene ring of **12** does not show such an effect.

The NOESY experiments on **8** show intense cross peaks between OMe and OCH_2, and between OMe and SCH_2CO with cross peak intensities of 0.37 and 0.17, respectively. These results show the proximity of OCH_2 and SCH_2CO units to the OMe unit and confirm the presence of an OMe group in the cavity of macrocyclic ring and thus the in-plane position of the *m*-phenylene and macrocyclic rings. Furthermore, NOESY experiments on **13** show the cross peaks between OCH_2 and ArH, and between SCH_2CO and ArH with cross peak intensities of 0.43 and 0.15, respectively. The appearance of a singlet for ArH and their high cross peak volumes further support the perpendicular placement of the *p*-phenylene ring with respect to the macrocyclic ring. Hence, in trithiocrownophanes **7**, **8** and **13**, the *m*-phenylene ring lies in plane and the *p*-phenylene ring acquires a position perpendicular to the macrocyclic ring. These results are further supported by molecular modelling.

The force field energy minimization [17] by DTMM 2.0 (Fig. 3) shows that in compounds **7** and **8**, the *m*-phenylene rings remain more or less in-plane with the mean plane of the macrocyclic ring and three thioether units are directed towards the cavity resulting in a triangle with three angles at 51 ± 0.1, 62 ± 0.5 and 67 ± 0.6° and three S–S distances at 6.57, 5.51 and 6.23 Å for **7** and 6.49, 5.51 and 6.24 Å for **8** (Table 2). In the compound **13**, the *p*-phenylene ring remains perpendicular to the mean plane of the macrocyclic ring. The S–S distance between two benzylic thioethers (7.09 Å) is much larger than the other two S–S distances (3.91 and 5.08 Å, Table 2).
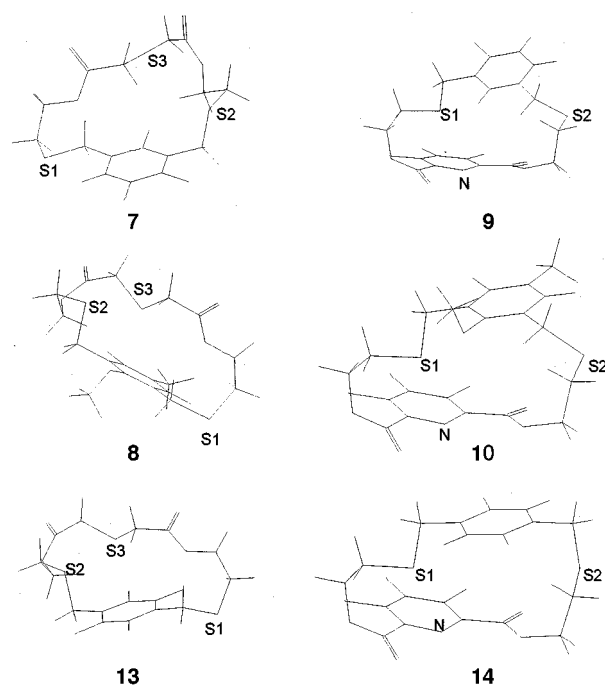
Fig. 3 Energy minimized (DTMM 2.0) structures of macrocycles **7–10**, **13** and **14**
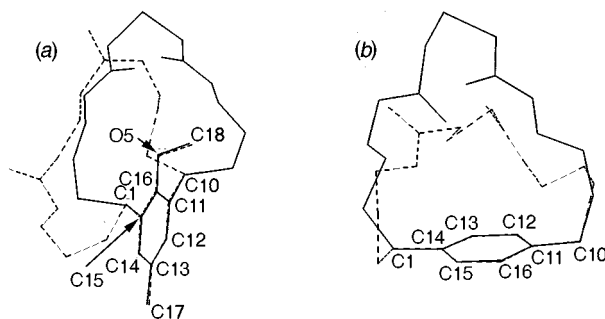
Fig. 4 Overlap of energy minimized conformations (– – –) and X-ray crystal structure (——) for crownophanes **8** (*a*) and **13** (*b*). Graphics drawn by SHELXTL-Plus 95.

It may be observed that the results of both X-ray and energy minimization studies are corroborative of in-plane and perpendicular positions of *m*-phenylene in **8** and *p*-phenylene in **13** but some contradictions are also revealed. In crownophane **8**, the crystal structure reveals that C10–S2 and O5–C18 bonds lie on one side and C1–S1 on the opposite side of the *m*-phenylene ring, whereas energy minimizations put C10–S2 and C1–S1 in one direction. This difference in the direction of C–S bonds causes the rest of the ring to be less extended than is observed in the X-ray structure [Fig. 4(*a*)]. Similarly, crownophane **13** exhibits a less extended conformation [Fig. 4(*b*)] by energy minimization than is observed by X-ray diffraction. These differences are not unexpected as the X-ray crystal structures are also dependent on lattice interactions and energy minimizations represent isolated molecules. However, both the studies, signifi-

Table 3 Cation extraction (%) profile of crownophanes **7–10**, **13** and **14**

Crownophane	Li$^+$	Na$^+$	K$^+$	Mg^{2+}	Ca^{2+}	Sr^{2+}	Ba^{2+}	Tl$^+$	Pb^{2+}	Ag$^+$	Ag$^+$/Pb^{2+}	Ag$^+$/Tl$^+$
7	0.016	—	0.04	—	0.07	—	0.09	0.09	0.39	67.30	172.6	747.8
8	—	—	—	—	0.027	—	0.074	—	0.75	73.38	97.84	—
13	—	0.05	—	—	0.02	0.11	—	0.09	1.06	57.2	53.96	635.6
9	0.086	0.092	0.01	0.065	0.022	0.064	0.074	0.25	0.10	60.28	602.8	241.1
10	0.084	0.064	0.021	0.025	0.033	0.039	0.031	4.24	0.76	82.34	108.34	19.4
14	0.064	0.03	0.04	0.03	0.063	0.07	0.074	1.51	15.2	71.61	4.71	47.4

cantly, lead to similar overall conformations of the phenylene rings with respect to the macrocyclic ring.

In crownophanes **9**, **10** and **14**, the appearance of OCH$_2$, SCH$_2$ and ArCH$_2$ ^{1}H NMR signals downfield of the corresponding signals in trithioether derivatives by 0.2–0.4, 0.1–0.3 and 0.1–0.2 ppm, respectively, points to their relatively rigid nature. The comparison of the ^{1}H NMR spectrum of 1:1 stoichiometric product **10** with the 2:2 stoichiometric product **15** shows ArCH$_2$ ($\Delta\delta$ +0.09) and SCH$_2$ ($\Delta\delta$ +0.20) signals downfield in the case of **10** and indicates a relatively more rigid structure for **10** than for its dimer **15**. In **14**, the OCH$_2$ signals appear upfield ($\Delta\delta$ −0.16) of those in **9** and **10**. So, unlike trithioether based crownophanes **7**, **8** and **13**, the pyridine based crownophanes **9**, **10** and **14** lack orderly placement of ^{1}H NMR signals and hence their conformational analysis could not be deduced from these data. However, force field energy minimizations (Fig. 3) show that in all the pyridine based macrocycles, either pyridine or the phenylene ring lies perpendicular to the plane of the macrocyclic ring. Again, in both **9** and **10**, the *m*-phenylene ring lies in the plane of the macrocyclic ring and the pyridine ring is more or less perpendicular to this plane. In the case of **14**, the pyridine ring is in the mean plane of the macrocyclic ring and the *p*-phenylene ring is perpendicular to it. Further analysis of the distances and angles between two thioether and one pyridine units shows that **9**, **10** and **14** have similar placement of two thioether units and pyridine N with respect to each other.

Binding characteristics
Extraction[18] and transport[19] studies. As the process of ligand facilitated transport of cations across a non-polar membrane has relevance to the development of separation techniques for cations, the extraction (complexation) and transport (complexation/decomplexation) profiles of macrocycles **7–10** and **13–14** towards Ag$^+$, Pb^{2+}, Tl$^+$, alkali metal cations (Li$^+$, Na$^+$, K$^+$) and alkaline earth cations (Mg^{2+}, Ca^{2+}, Sr^{2+}, Ba^{2+}) by using chloroform as an apolar membrane have been determined. In thioether based macrocycles, 1:1 and/or 2:2 stoichiometric complexation is facilitated in the solid phase but in the solution phase the 1:1 complexations are more pronounced. So for discussion of all the extraction and transport results 1:1 stoichiometric complexation of macrocycles with cations has been assumed.

The macrocycles **7**, **8** and **13** (3 × −S−) and **9**, **10** and **14** (2 × −S− and PyN) possess three soft ligating sites and two relatively non-participating ester oxygens. The discussion of the ionophore character of these macrocycles is primarily based on three soft ligating sites as, in their ^{13}C NMR titrations with Ag$^+$, the participation of only three soft sites is evident.

These macrocycles with the exception of **14** show significant Ag$^+$/Pb^{2+} extraction selectivity (Table 3, Fig. 5). The macrocycle **7** extracts 172 times more silver picrate (67.30%) than Pb^{2+} (0.39%) and **8** shows relatively enhanced extraction of both Ag$^+$ (73.3%) and Pb^{2+} (0.76%) resulting in lowering of Ag$^+$ *vs.* Pb^{2+} selectivity to 98. The alkali, alkaline earth and Tl$^+$ cations are extracted only marginally. *p*-Crownophane **3** shows lowering in both extraction of Ag$^+$ (57.2%) and Ag$^+$ *vs.* Pb^{2+} selectivity. The *m*-phenylene crownophanes **7** and **8** have similar conformations, but the higher degree of extraction of Ag$^+$ and
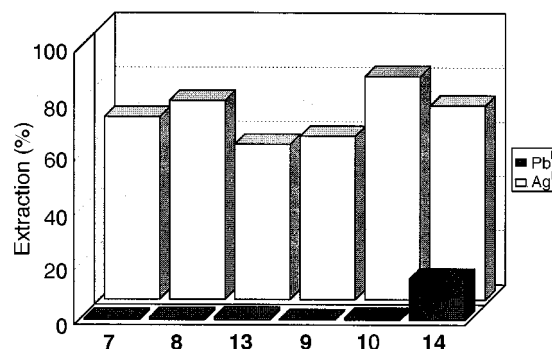
Fig. 5 Extraction (%) of Ag^{I} and Pb^{II} by crownophanes **7–10**, **13** and **14**

Pb^{2+} by **8** in comparison with **7** could be attributed to the cooperative participation of the methoxy group in complexation with cations. As expected, the methoxy unit shows better interaction with dipositive Pb^{2+} than monopositive Ag$^+$ and therefore Ag$^+$/Pb^{2+} selectivity in **8** is lowered in comparison with **7**. In **13**, the *p*-phenylene ring places the two thioether units relatively far apart and causes lower extraction and selectivity for Ag$^+$.

In the three-dimensional structure of the macrocycle **9** the pyridine ring is perpendicular to the *m*-phenylene ring. But PyN is placed only 5 Å units away from both the thioether −S− atoms and this arrangement leads to 602 times more extraction of Ag$^+$ (60.28%) than Pb^{2+} (0.1%, Table 3). The conformation of macrocycle **10** is similar to that of **9**, but its cavity is filled by the methoxy group. It seems that the methoxy group participates in complexation and thus macrocycle **10** shows increased extraction of Ag$^+$, Pb^{2+} and Tl$^+$ by nearly 1.4, 7.6 and 16 times, respectively, in comparison with **9**, thereby lowering the Ag$^+$/Pb^{2+} selectivity to 108. In the macrocycle **14**, the pyridine ring is in the plane of the macro-ring and is more available for complexation than in the case of **9** and **10** and shows some increase in extraction of Ag$^+$ (71.61%), but extraction of Pb^{2+} is significantly increased to 15.2% from only 0.10% in the case of **9**. As a result, **14** shows only a marginal Ag$^+$ *vs.* Pb^{2+} selectivity (Fig. 5).

Amongst these designs, *m*-phenylene derivatives **7** and **9** show the highest degree of binding selectivity for Ag$^+$ though their extraction character is lower. In macrocycles **8** and **10**, the possible participation of the methoxy group increases the extraction of all the cations but their three-dimensional arrays include a much more pronounced increase in the extraction of Pb^{2+} and Tl$^+$, and Ag$^+$ selectivities are lowered. Furthermore, both *p*-crownophane derivatives **13** and **14** show much lower Ag$^+$/Pb^{2+} selectivity than their *m*-phenylene counterparts **7** and **9**.

The transport rates for Pb^{2+} picrate could not be determined because of its significant leakage across chloroform.[20] Since amongst the cations studied here, after Ag$^+$, the most efficiently transported cation is Tl$^+$, selectivities have been presented with respect to Tl$^+$ and for other cations these are fairly high (Table 4). The trithioether macrocycles **7**, **8** and **13** transport Ag$^+$ at similar rates. But **8**, in which the methoxy group can interact with Tl$^+$, shows the lowest selectivity. Amongst pyridine based

Table 4 Transport (10^{-8} mol/24 h) profile of crownophanes **7–10**, **13** and **14**

Crownophane	Li$^+$	Na$^+$	K$^+$	Mg^{2+}	Ca^{2+}	Sr^{2+}	Ba^{2+}	Tl$^+$	Ag$^+$	Ag$^+$/Tl$^+$
7	76.7	118.7	26.0	30.4	40.8	43.7	51.8	88.3	3266.2	37
8	50.5	106.8	68.6	71.7	55.4	66.2	63.6	128.2	3110.3	24
13	13.6	13.4	15.1	14.2	7.2	8.5	18.4	44.0	3411.1	78
9	9.21	7.63	11.6	5.08	6.00	3.60	3.35	43.71	4509.6	103
10	14.6	14.47	11.1	10.78	34.9	10.3	4.29	297.0	1279.1	4.3
14	8.19	16.23	21.3	12.72	13.7	11.8	31.2	227.7	1498.4	6.6

Table 5 Metal picrate induced ^{13}C NMR coordination shifts ($\Delta\delta_C$) of crownophanes **7**, **8** and **13**

	Me	SCH$_2$	SCH$_2$	SCH$_2$	OMe	OCH$_2$	ArC	ArC	ArC	ArC–O	C=O
7·Ag$^+$	—	1.78	1.80	0.88	—	−0.74	0.78	0.08	0.63	−0.68	0.40
7·Pb^{2+}	—	−0.01	−0.05	0.48	—	0.22	−0.01	0	−0.05	0	0.02
7·Sr^{2+}	—	−0.01	0	0.51	—	0.23	0	0.01	−0.05	−0.01	0.05
7·Na$^+$	—	0.02	−0.01	0.02	—	0.22	0	−0.01	−0.06	0.02	0.03
8·Ag$^+$	−0.10	2.86	2.33	1.70	0.19	−0.99	0.28	−0.19	0.35	—	−0.01
8·Pb^{2+}	0.02	0.04	0.04	−0.54	0.02	0.03	0.06	0.02	0.03	—	0.05
8·Sr^{2+}	0.03	0.05	0.06	0.07	−0.17	0.05	0.03	0.02	0.05	—	0.09
8·Na$^+$	0.05	0.05	0.06	0.05	−0.77	0.04	0.03	0.02	—	—	—
13·Ag$^+$	—	2.09	0.99	1.17	—	−0.08	0.61	—	—	−0.27	0.51
13·Pb^{2+}	—	0.03	0.02	−0.24	—	0.02	0.02	—	—	0.02	0.03
13·Sr^{2+}	—	0.04	0.06	−0.23	—	0.04	0.03	—	—	0.01	0.05
13·Na$^+$	—	0.02	−0.02	−0.23	—	0.02	0.01	—	—	−0.01	0.04
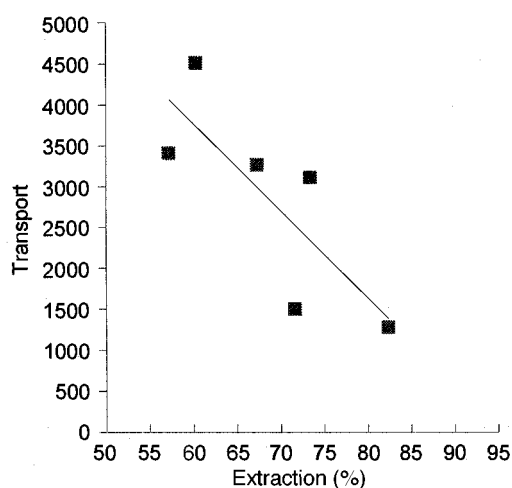
Fig. 6 Plot of extraction (%) *vs.* transport of crownophanes **7–10**, **13** and **14**

ionophores, **9** transports Ag$^+$ most efficiently and is the best ionophore with the highest efficiency and selectivity amongst all the six macrocycles discussed here. In parallel with the extraction results, **10** and **14**, which show highest extraction for Tl$^+$, also show the highest transport efficiencies and lead to only marginal Ag$^+$/Tl$^+$ selectivities. Furthermore, amongst all these compounds, the crownophanes **8** and **10** bearing methoxy units show the lowest selectivities which further confirms the more effective participation of the methoxy group in binding with cations other than Ag$^+$. Also, the comparison of extraction and transport results of Ag$^+$ (Fig. 6) shows that with these macrocycles more than 60% extraction of Ag$^+$ leads to its lower transport rates, whereas for Tl$^+$ and other cations, the increased extraction is coupled with increased transport rates. Evidently, in the case of **10** and **14**, the slower decomplexation of the more stable macrocycle–Ag$^+$ picrate complexes may be at least partially responsible for lower transport rates.

Complexation studies through ^{13}C NMR spectroscopy

The comparison of ^{13}C NMR spectra of macrocycles with those of their 1:1 stoichiometric mixtures with metal picrates gives significant information about the complexation character of individual ligating sites in these macrocycles.

The *m*-phenylene crownophanes, **7** and **8**, show a significant downfield shift for three SCH$_2$ carbon signals. This shift is more pronounced in **8**, which has been found to be a better complexing agent than **7** in extraction experiments (Table 5). The participation of OMe is also evident from the downfield shift of the OMe NMR signal. The OCH$_2$ signals also experience the effect of Ag$^+$ binding and are shifted upfield. This could be attributed to the high electron density of Ag$^+$ and its proximity to OCH$_2$ units. In macrocycle **13**, again SCH$_2$ signals are shifted downfield but OCH$_2$ remains almost at the same position. The analysis of the DTMM based conformation of **13** shows that in the **13**–Ag$^+$ complex, Ag$^+$ should be placed in line with *p*-phenylene thioether units and would be quite far from the OCH$_2$.

The addition of Ag$^+$ picrate to a solution of crownophane **9** causes separation of a solid product and so NMR monitoring of the complexation could not be carried out. But in the case of **10** (Table 6), as expected, SCH$_2$ and OCH$_3$ signals are shifted downfield and the OCH$_2$ signal is shifted upfield. Also, the participation of the OMe unit is more effective in **10** than in **8**. However, due to the difficulty in differentiation of aryl and pyridine signals, the participation of pyridine could not be determined.

In conclusion, *m*-phenylene (**7–10**) and *p*-phenylene (**13–14**) based crownophanes offer three soft coordinating sites (3 × S or 2 × S and 1 N) conducive to complexation with Ag$^+$ and the steric restrictions imposed by *m*- and *p*-phenylene rings restrict 2:1 (L:M) sandwich complexation required for complexation with the soft Pb^{2+} cation. These structural features induce high Ag$^+$/Pb^{2+} selectivities. But in crownophanes **8** and **10**, the presence of a hard ether ligating unit adversely affects the Ag$^+$/Pb^{2+} selectivity.

Experimental

Table 6 Metal picrate induced ^{13}C NMR coordination shifts ($\Delta\delta_C$) of crownophanes **9**, **10** and **14**

	SCH$_2$	SCH$_2$	OCH$_3$	OCH$_2$	ArC	ArC	ArC	ArC	PyC	PyC	PyC−N	C=O
9·Pb^{2+}	0.05	—	—	−0.04	0.03	−0.01	—	—	−0.02	0.03	−0.02	0.03
9·Tl^{+}	0.17	—	—	−0.22	0.07	0.02	—	−0.12	−0.08	0.06	−0.06	−0.04
9·Na^{+}	0.05	—	—	−0.04	0.06	0.01	0.22	—	−0.02	—	0.43	—
9·Sr^{2+}	0.06	—	—	−0.03	0.01	—	—	0.01	—	0.03	−0.02	0.04
10·Ag^{+}	2.35	1.44	1.42	−3.12	1.64	0.24	—	−1.90	1.37	—	—	—
10·Pb^{2+}	0.01	0.00	0.01	−0.01	—	0.03	−0.02	0.03	−0.01	—	0.01	0.39
10·Tl^{+}	0.37	—	−0.04	−0.72	0.66	0.62	0.66	—	0.36	—	0.47	−0.35
10·Na^{+}	−0.05	−0.01	−0.03	−0.01	0.04	0.04	0.03	—	0.01	—	−0.01	—
10·Sr^{2+}	−0.01	−0.01	—	0.02	−0.20	−0.03	—	0.01	—	−0.02	—	—
14·Ag^{+}	3.85	0.30	—	−0.06	—	0.13	—	—	0.62	—	0.31	—
14·Pb^{2+}	0.01	−0.01	—	−0.08	0.03	—	—	−0.01	0.03	—	−0.04	—
14·Tl^{+}	—	—	−0.26	—	−0.03	−0.03	—	—	—	—	—	—
14·Na^{+}	—	0.01	−0.26	—	−0.08	0.03	—	—	−0.02	—	−0.04	0.25
14·Sr^{2+}	—	0.01	−0.24	—	−0.06	—	—	—	—	0.14	—	0.20

recorded on a Shimadzu UV-240 spectrophotometer. Elemental analysis of solid samples was performed at the microanalytical laboratory RSIC, Chandigarh.

Synthesis of diols 3, 4 and 12

General procedure. A solution of 1,3-bis(bromomethyl)-benzene (**1**) (1.00 g, 3.7 mmol) and 2-mercaptoethanol (0.74 g, 10.11 mmol) in DMF (dry, 50 cm^3) containing anhydrous K$_2$CO$_3$ (2.65 g, 18.96 mmol) and tetrabutylammonium hydrogen sulfate (Bu$_4$N$^+$HSO$_4^−$) was stirred. After completion of the reaction (TLC, 8 h), the solid suspension was filtered and the residue was washed with ethyl acetate (10 cm^3). The combined filtrate was distilled under vacuum. The residue was chromatographed on a silica gel column using hexane–ethyl acetate (gradient elution 10:1→1:1) as eluents to isolate diol **3**. Similarly, reaction of 1,3-bis(bromomethyl)-2-methoxy-5-methyl-benzene (**2**) and 1,4-bis(bromomethyl)benzene (**11**) with 2-mercaptoethanol gave diols **4** and **12**.

1,3-Bis(2-hydroxyethylthiomethyl)benzene (**3**) (80%), liquid; δ_H(CDCl$_3$) 2.58 (4H, t, J 6.2, 2 × SCH$_2$), 3.61 (4H, t, J 6.2, 2 × OCH$_2$), 3.70 (4H, s, SCH$_2$), 7.15–7.33 (4H, m, ArH); δ_C(CDCl$_3$) 36.43 (t, SCH$_2$), 41.15 (t, SCH$_2$), 61.54 (t, OCH$_2$), 127.53 (d, ArCH), 128.70 (d, ArCH), 129.25 (d, ArCH), 138.46 (s, ArC); ν_{max}(KBr)/cm^{-1} 3400 (OH); m/z 258 (M$^+$).

1,3-Bis(2-hydroxyethylthiomethyl)-2-methoxy-5-methyl-benzene (**4**) (80%), liquid; δ_H(CDCl$_3$) 2.29 (3H, s, Me), 2.63 (4H, t, J 6.0, 2 × SCH$_2$), 3.67 (4H, t, J 6.0, 2 × OCH$_2$), 3.72 (4H, 2 × SCH$_2$), 3.84 (3H, s, OCH$_3$), 7.57 (2H, s, ArH); δ_C(CDCl$_3$, DEPT-135) 20.65 (+ve, CH$_3$), 29.61 (−ve, SCH$_2$), 34.18 (−ve, SCH$_2$), 60.68 (−ve, OCH$_2$), 62.35 (+ve, OCH$_3$), 130.44 (+ve, ArCH), 131.11 (absent, ArC), 134.01 (absent, ArC), 154.22 (absent, ArC−O); ν_{max}(KBr)/cm^{-1} 3400 (OH); m/z 302 (M$^+$).

1,4-Bis[(2-hydroxyethylthio)methyl]benzene (**12**) (85%), mp 58 °C (CHCl$_3$); δ_H(CDCl$_3$) 2.62 (4H, t, J 6.0, 2 × SCH$_2$), 3.63 (4H, t, J 6.0, 2 × OCH$_2$), 3.70 (4H, s, SCH$_2$), 7.27 (4H, s, ArH); δ_C(CDCl$_3$, DEPT-135) 34.21 (−ve, SCH$_2$), 41.26 (−ve, SCH$_2$), 60.32 (−ve, OCH$_2$), 129.11 (+ve, ArCH), 137.12 (absent, ArC); ν_{max}(KBr)/cm^{-1} 3300 (OH); m/z 258 (M$^+$) (Found: C, 55.45; H, 6.87. C$_{12}$H$_{18}$O$_2$S$_2$ requires C, 55.81; H, 6.97%).

Synthesis of crownophanes 7, 8 and 13

General procedure. Diol **4** (1.00 g, 3.9 mmol), KF (anhyd.) and a catalytic amount of Bu$_4$N$^+$HSO$_4^−$ (10 mg) were dissolved in dry dichloromethane (100 cm^3) and the reaction mixture was stirred at room temperature. Thiodiglycolyl dichloride (0.73 g, 3.87 mmol) dissolved in dichloromethane (50 cm^3) was added dropwise, over 0.5 h. After completion of the reaction (TLC, 7 h), the solid suspended was filtered off and was washed with ethyl acetate (2 × 10 cm^3). The combined filtrate was distilled off. The crude reaction product was chromatographed on a silica gel column using hexane–ethyl acetate (gradient elution

10:1→1:1) as eluents to isolate **9**. Similarly cyclocondensation of diols **5** and **7** with thiodiglycolyl chloride gave macrocycles **10** and **11**.

6,12-Dioxa-3,9,15-trithia-1(1,3)-benzenacyclohexadeca-phane-7,11-dione (**7**) (40%), liquid; δ_H(CDCl$_3$) 2.64 (4H, t, J 7.0, 2 × SCH$_2$), 3.39 (4H, s, 2 × SCH$_2$CO), 3.76 (4H, s, 2 × SCH$_2$Ar), 4.20 (4H, t, J 7.0, 2 × OCH$_2$), 7.23–7.35 (4H, m, ArH); δ_C(CDCl$_3$) 28.84 (t, SCH$_2$), 34.03 (t, SCH$_2$), 36.05 (t, SCH$_2$), 64.42 (t, OCH$_2$), 127.79 (d, ArCH), 129.40 (d, ArCH), 129.69 (d, ArCH), 138.15 (s, ArC), 169.21 (s, C=O); ν_{max}(CHCl$_3$)/cm^{-1} 1750, 1740 (C=O); m/z 372 (M$^+$).

1^2-Methoxy-1^5-methyl-6,12-dioxa-3,9,15-trithia-1(1,3)-benzenacyclohexadecaphane-7,11-dione (**8**) (35%); mp 100 °C (CH$_3$CN); δ_H(CDCl$_3$) 2.32 (3H, s, CH$_3$), 2.57 (4H, deformed t, J 6.8, 2 × SCH$_2$), 3.33 (4H, s, 2 × SCH$_2$), 3.69 (3H, s, OCH$_3$), 3.73 (4H, s, 2 × SCH$_2$), 4.19 (4H, deformed t, J 6.8, 2 × OCH$_2$), 7.13 (2H, s, ArH); δ_C(CDCl$_3$) 20.89 (q, CH$_3$), 28.23 (t, SCH$_2$), 29.12 (t, SCH$_2$), 33.62 (t, SCH$_2$), 62.46 (q, OCH$_3$), 64.56 (t, OCH$_2$), 130.63 (d, ArCH), 130.96 (s, ArC), 134.86 (s, ArC), 154.86 (s, ArC−O), 169.10 (s, C=O); ν_{max}(KBr)/cm^{-1} 1743 (C=O); m/z 416 (M$^+$, 12%) (Found: C, 52.10; H, 5.80. C$_{18}$H$_{24}$O$_5$S$_3$ requires C, 51.92; H, 5.76%).

6,12-Dioxa-3,9,15-trithia-1(1,4)-benzenacyclohexadeca-phane-7,11-dione (**13**) (10%), mp 62 °C (CH$_3$CN); δ_H(CDCl$_3$) 2.54 (4H, deformed t, J 6.0, SCH$_2$), 3.20 (4H, s, SCH$_2$), 3.70 (4H, s, SCH$_2$), 3.78 (4H, deformed t, J 6.0, OCH$_2$), 7.33 (4H, s, ArH); δ_C(CDCl$_3$) 28.37 (t, SCH$_2$), 34.93 (t, SCH$_2$), 36.26 (t, SCH$_2$), 64.09 (t, OCH$_2$), 129.31 (d, ArCH), 137.46 (s, ArC), 169.09 (s, C=O); ν_{max}(KBr)/cm^{-1} 1742 (C=O); m/z 372 (M$^+$) (Found: C, 51.76; H, 5.20. C$_{16}$H$_{20}$O$_4$S$_3$ requires C, 51.61; H, 5.37%).

Synthesis of crownophanes 9, 10, 14 and 15

General procedure. Diol **3** (1 g, 3.9 mmol), K$_2$CO$_3$ (anhyd.) and a catalytic amount of Bu$_4$N$^+$HSO$_4^−$ (10 mg) were dissolved in dry dichloromethane (100 cm^3) and the reaction mixture was stirred at room temperature. Pyridine-2,6-dicarbonyl dichloride (0.73 g, 3.9 mmol) solution in dichloromethane (dry, 50 cm^3) was added dropwise, over 0.5 h. After completion of the reaction (TLC, 7 h), the suspension was filtered off and the solid residue was washed with ethyl acetate (2 × 10 cm^3). The combined filtrate was distilled off. The crude reaction product was chromatographed on a silica gel column using hexane–ethyl acetate mixtures as eluents to isolate a white compound **9**.

6,10-Dioxa-3,13-dithia-1(1,3)-benzena-8(2,6)-pyridinacyclo-tetradecaphane-7,9-dione (**9**) (35%), mp 147 °C (CHCl$_3$); δ_H(CDCl$_3$) 2.67 (4H, t, J 6.0, 2 × SCH$_2$), 3.91 (4H, s, 2 × SCH$_2$), 4.59 (4H, t, J 6.0, 2 × OCH$_2$), 7.25–7.34 (3H, m, ArH), 7.93 (1H, s, ArH), 8.03 (1H, t, J 7.8, PyH), 8.37 (2H, d, J 7.8, PyH); δ_C(CDCl$_3$, DEPT-135) 27.81 (−ve, SCH$_2$), 36.13 (−ve, ArSCH$_2$), 68.44 (−ve, OCH$_2$), 127.59 (+ve,

PyCH), 128.60 (+ve, ArCH), 129.44 (+ve, ArCH), 132.91 (+ve, ArCH), 137.52 (+ve, ArCH), 138.02 (absent, ArC), 148.54 (absent, PyC–N), 165.27 (absent, C=O); ν_{max}(KBr)/cm^{-1} 1715 (C=O); m/z 389 (M$^+$, 20%) (Found: C, 58.42; H, 4.31; N, 3.41. $C_{19}H_{19}NO_4S_2$ requires C, 58.61; H, 4.88; N, 3.59%).

1^2-Methoxy-1^5-methyl-6,10-dioxa-3,13-dithia-1(1,3)-benzena-8(2,6)-pyridinacyclotetradecaphane-7,9-dione (10) (35%), mp 128–132 °C (CHCl$_3$); δ_H(CDCl$_3$) 2.29 (3H, s, CH$_3$), 2.87 (4H, t, J 6.0, 2 × SCH$_2$), 3.72 (3H, s, OMe), 3.84 (4H, s, 2 × SCH$_2$), 4.41 (4H, t, J 6.0, 2 × OCH$_2$), 7.09 (2H, s, ArH), 7.94–8.01 (1H, m, PyH), 8.24 (2H, s, J 8.0, PyH); δ_C(CDCl$_3$) 20.84 (q, CH$_3$), 29.57 (t, SCH$_2$), 30.74 (t, SCH$_2$), 62.37 (q, OCH$_3$), 65.85 (t, OCH$_2$), 127.66 (d, PyCH), 130.76 (d, ArCH), 134.40 (d, PyCH), 137.96 (s, ArC), 148.20 (s, PyC–N), 155.54 (s, ArC–O), 164.60 (s, C=O); m/z 433 (M$^+$, 13%) (Found: C, 57.74; H, 5.30; N, 3.30. $C_{21}H_{23}NO_5S_2$ requires C, 58.01; H, 5.31; N, 3.23%).

6,10-Dioxa-3,13-dithia-1(1,4)-benzena-8(2,6)-pyridinacyclotetradecaphane-7,9-dione (14) (25%), mp 197 °C (CHCl$_3$); δ_H(CDCl$_3$) 2.62 (4H, t, J 6.6, 2 × SCH$_2$), 3.85 (4H, s, 2 × SCH$_2$), 4.44 (4H, t, J 6.6, 2 × OCH$_2$), 7.30 (4H, s, ArH), 8.03 (1H, t, J 8.0, PyH), 8.32 (2H, d, J 8.0, PyH); δ_C(CDCl$_3$) 28.75 (t, SCH$_2$), 36.02 (t, SCH$_2$), 65.91 (t, OCH$_2$), 128.17 (d, PyCH), 129.44 (d, ArCH), 137.16 (s, ArC), 148.25 (s, PyC–N), 164.60 (s, C=O); m/z 389 (M$^+$) (Found: C, 58.30; H, 4.54; N, 3.30. $C_{19}H_{19}NO_4S_2$ requires C, 58.61; H, 4.88; H, 3.59%).

1^2,15^2-Dimethoxy-1^5,15^5-dimethyl-6,10,20,24-tetroxa-3,13,17,27-tetrathia-1,15(1,3)-dibenzena-8,22(2,6)-dipyridinacyclooctaicosophane-7,9,21,23-tetrone (15) (10%), mp 180 °C (CHCl$_3$); δ_H(CDCl$_3$) 2.24 (3H, s, CH$_3$), 2.69 (4H, t, J 6.6, 2 × SCH$_2$), 3.79 (3H, s, OMe), 3.87 (4H, s, 2 × SCH$_2$), 4.44 (4H, t, J 6.6, 2 × OCH$_2$), 7.08 (2H, s, ArH), 7.97 (1H, t, J 8.0, PyH), 8.30 (2H, d, J 8.0, PyH); m/z (FAB) 867 (M$^+$ + 1).

X-Ray structure analysis of crownophanes 8 and 13

All intensity data measurements were carried out on a Siemens P4 four circle diffractometer with graphite monochromatic Mo-Kα radiation ($\lambda = 0.710\ 69$ Å). All structures were solved and refined using the SHELXTL software[20] package on a Siemens Nixdorf computer. Crystals of 8 and 13 suitable for X-ray diffraction work were obtained by recrystallization from acetonitrile. The unit cell parameters were determined from a least squares fit of setting angles of 25 reflections in the range $20 \leqslant 2\theta \leqslant 25°$. Three standard reflections were measured every 100 reflections and showed no significant intensity variation during the data collection. The data were corrected for Lorentz and polarization effects. No absorption corrections were applied. The structures were solved by the direct methods. Full matrix least squares refinement was employed with anisotropic thermal parameters for the non-hydrogen atoms. The hydrogen atoms placed at calculated positions were refined isotropically with fixed thermal parameters and included in structure factor calculations. Crystal data and parameters for data collection and refinements are summarized in Table 7. Full crystallographic details, excluding structure factor tables, have been deposited at the Cambridge Crystallographic Data Centre (CCDC). For details of the deposition scheme, see 'Instructions for Authors', *J. Chem. Soc.*, *Perkin Trans. 2*, available *via* the RSC Web page (http://www.rsc.org/authors). Any request to the CCDC for this material should quote the full literature citation and the reference number 188/121.

Extraction measurements[18]

For the extraction experiments, metal picrate solutions (0.01 mol dm^{-3}) were prepared in deionized distilled water. The solutions of macrocycles (0.01 mol dm^{-3}) were prepared in chloroform (AR grade).

An aqueous solution (2 cm^3) of metal picrate (0.01 mol dm^{-3})

Table 7 Crystal data collection and refinement parameters for crownophanes 8 and 13

Compounds	8	13
Empirical formula	$C_{18}H_{24}O_5S_3$	$C_{16}H_{20}O_4S_3$
M	416.55	372.50
Crystal system	Monoclinic	Monoclinic
Space group	$P2_1/n$	$P2_1/c$
a/Å	13.433(1)	16.333(1)
b/Å	9.941(1)	8.670(1)
c/Å	14.977(1)	13.005(1)
β/°	103.45(10)	98.69(10)
U/Å^3	1945.1(3)	1820.5(3)
Z	4	4
Crystal size/mm	$0.2 \times 0.3 \times 0.2$	$0.3 \times 0.3 \times 0.2$
μ(Mo-Kα)/cm^{-1}	0.710 73	0.710 73
$2\theta_{max}$/°	45	35
No. of measured reflections	2487	1446
No. of unique reflections	2359	1133
R_{int}	0.0291	0.0208
No. of observations $[I > 3\sigma(I)]$	2285	1133
No. of variables	235	208
Residuals: R	0.0356	0.0320
Max. and min. residual	0.384, −0.263	0.177, −0.197
Electron density/e Å^{-3}		
Goodness of fit (GOOF)	1.056	1.172

and a chloroform solution (2 cm^3) of the macrocycle (0.01 mol dm^{-3}) were shaken in a cylindrical tube closed with a septum for 5 min and kept at 27 ± 1 °C for 3–4 h. An aliquot of the chloroform layer (1 cm^3) was withdrawn with a syringe and diluted with acetonitrile to 10 cm^3. The UV absorption was measured against CHCl$_3$–CH$_3$CN (1:9) solution at 374 nm. Extraction of metal picrate has been calculated as the percentage of metal picrate extracted in the chloroform layer and the values reported here are the mean of three independent measurements which were within ±2% error (Table 2).

Transport measurements[19]

The transport experiments were carried out at constant temperature (27 ± 1 °C) in a cylindrical glass cell consisting of outer and inner jackets by using (*i*) metal picrate (0.01 mol dm^{-3}) in water (3 cm^3) in the inner phase; (*ii*) water (10 cm^3) in the outer phase; (*iii*) ligand (10 mmol dm^{-3}) in a chloroform layer (15 cm^3) with stirring (150 ± 5 rpm) at 27 ± 1 °C. After stirring for 6 h the picrates transported in the aqueous receiving phase were determined from the UV absorptions at 355 nm. Each value is a mean of three experiments which are consistent ±10% (Table 3). Before determining the transport rates, blank experiments were performed in the absence of the carrier macrocycle in the chloroform layer to check the leakage of metal picrates. Under the conditions given for the transport experiments, in the absence of crownophanes, metal picrates (except Pb^{2+} picrate) are not transported to the receiving phase. However, Pb^{2+} picrate shows significant transport and results for crownophane induced transport of Pb^{2+} are not reliable and, therefore transport of Pb^{2+} was not determined.

DTMM 2.0 programme[17]

The programme was used as provided by the company, without any further modification. The programme DTMM 2.0 uses molecular mechanics potentials and their force fields similar to those in ref. 21. These include bond stretching potential, bong angle deformation potential, periodic torsional barrier potential and non-bonding interactions for non-bonded atom pairs. For every bond, six variables, bond length (1), bond rotation (1) and fragment orientation (4) are minimized. All variables are treated independently using a simple line search algorithm with quadratic interpolation. It provides facilities for conformational space hunting, charge calculations and hydrogen bonding.

References

1 Part 17: S. Kumar, J. Kaur and H. Singh, *J. Incl. Phenom. Mol. Recogn.*, in the press. Preliminary communication: S. Kumar, V. Bhalla, P. Singh and H. Singh, *Tetrahedron Lett.*, 1996, **53**, 3495.
2 S. Kumar, M. S. Hundal, N. Kaur, R. Singh, H. Singh, G. Hundal, M. M. Ripoll and J. S. Aparicio, *J. Org. Chem.*, 1996, **61**, 7819.
3 S. Kumar, I. Kaur and H. Singh, *Indian J. Chem., Sect. A*, 1994, **33**, 412.
4 S. Kumar, N. Kaur and H. Singh, *Tetrahedron*, 1996, **52**, 13 483.
5 S. Kumar, N. Kaur and H. Singh, *Tetrahedron*, 1997, **53**, 10 841.
6 S. Kumar, V. Bhalla and H. Singh, *Bioorg. Med. Chem. Lett.*, 1995, **5**, 1917.
7 H. Tsukube, J. Venishi, N. Kojima and O. Yanemitsn, *Tetrahedron Lett.*, 1995, **36**, 2257.
8 T. Nabeshima, H. Furusawa and Y. Yano, *Angew. Chem., Int. Ed. Engl.*, 1994, **33**, 1750.
9 T. Nabeshima, H. Furusawa, N. Tsukada, T. Shinnai, T. Haruyama and Y. Yano, *Heterocycles*, 1995, 655.
10 T. Nabeshima, N. Tsukada, K. Nishijima, H. Oshiro and Y. Yano, *J. Org. Chem.*, 1996, **61**, 4342.
11 H. Hismoto, E. Nakagawa, K. Nagatsuka, Y. Abe, S. Sato, D. Siswanta and K. Suzuki, *Anal. Chem.*, 1995, **67**, 1315.
12 D. Siswanta, K. Nagatsuka, H. Yamada, K. Kumakura, H. Hisamoto, Y. Scichi, K. Toshima and K. Suzuki, *Anal. Chem.*, 1996, **68**, 4166.
13 T. Nabeshima, K. Nishijima, N. Tsukada, H. Furusawa, T. Hosoya and Y. Yano, *J. Chem. Soc., Chem. Commun.*, 1992, 1092.
14 J. Casabo, T. Flor, M. N. Stuart, H. A. Jenkins, J. C. Lockhart, S. J. Loeb, I. Romero and F. Texidor, *Inorg. Chem.*, 1995, **34**, 5410.
15 F. Texidor, M. A. Flores, L. Eschriche, G. Vinas and J. Cassabo, *J. Chem. Soc., Chem. Commun.*, 1994, 963.
16 Chemical shift variations for these compounds are within $\delta \pm 0.02$.
17 M. J. C. Crabbe and J. R. Appleyard, Desktop Molecular Modeller 2.0, Oxford Electronic Publishing, Oxford, 1991.
18 (*a*) S. S. Moore, T. L. Tarnowski, M. Newcomb and D. J. Cram, *J. Am. Chem. Soc.*, 1977, **99**, 6398; (*b*) K. E. Koeing, G. M. Lehn, P. Stuckler, T. Kaneda and D. J. Cram, *J. Am. Chem. Soc.*, 1979, **101**, 3553.
19 (*a*) K. Maruyama, H. Tsukube and T. Akai, *J. Am. Chem. Soc.*, 1980, **102**, 3246; (*b*) K. Maruyama, H. Tsukube and T. Akai, *J. Chem. Soc., Dalton Trans.*, 1981, 1486.
20 G. M. Sheldrick, SHELXTL-PC version 5.03, Siemens Analytical Instruments Inc., Madison, WI, 1995.
21 J. G. Vinter, A. Davis and M. R. Saunders, *J. Comput. Aided Mol. Design*, 1987, **1**, 31.